Static And Dynamic Analysis Of A Ball Mill For The Gold Mining Industry

José L. Serna-Landivar[1*], Daniela M. Anticona-Valderrama[2], Manuel López Miranda[3], Maria Y. Garcia-Alvarez[4], Jennifer Korall De la Cruz-Garcia[4], and William C. Algoner[5]

[1] *Universidad Científica del Sur, Lima, Perú*
[2] *Universidad Privada del Norte, Lima, Perú*
[3] *Universidad Ricardo Palma; Lima, Perú*
[4] *Universidad Tecnológica del Perú, Lima, Perú*
[5] *Universidad Continental, Escuela de Posgrado, Lima, Perú*
[*] *Corresponding author. E-mail: jsernal@cientifica.edu.pe*

Received: Dec. 16, 2025; Accepted: Apr. 13, 2026

This study deals with the structural analysis of a ball mill designed for small-scale gold mining operations, which is crucial in ore crushing, focusing on the dynamic and static forces that affect its performance during operations. A pre-experimental study of the main body was performed using finite element analysis in ANSYS software. Static analysis provided information on deformations, stresses, and safety factors, whereas modal analysis identified the natural frequencies and vibration modes. In addition, harmonic analysis was performed to evaluate the deformations and stresses induced by sinusoidal forces generated by fluctuating grinding loads. The results indicate that the natural vibration frequencies are 261.44 and 277.64 Hz for modes 4 and 5, respectively. Mode 4 presents circumferential behavior, in which alternating deformations are observed along the shell of the cylinder. On the other hand, mode 5 corresponds to an axial mode, characterized by vibrations predominantly along the longitudinal axis of the mill. The main conclusion is that the ball mill, intended for small-scale mining applications, was designed to operate safely under established speed and operating load parameters.

Keywords: Ball Mill; Static Analysis; Modal Analysis; Harmonic Analysis; FEA

http://dx.doi.org/10.6180/jase.202609_32.060

1. Introduction

Grinding is an industrial process that accounts for a large proportion of the mineral processing industry [1]. Ball mill grinding machines are the leading mining equipment used in mineral concentrator plants. The rotational speed of the ball mill depends on the shell diameter, as stated in Yoshida et al. [2] and Banisi and Hadizadeh [3]; however, it is crucial to adapt this speed to the specific conditions of each process. The main part of the mill is a rotating drum with horizontal positions, and the liner is located on the inner wall of the drum, including the entire inner surface of the mill shell and the inner faces of the ends on both sides. When the ball mill is operating, the ore particles enter from one end through the chute connected to the trunnion feed into the drum and are repeatedly impacted by steel balls against the liners until the ore slurry is of a suitable size and finally exits from the other end of the mill shell through the exit trunnion.

Ball mills have benefits owing to their simple design, stable operating performance, and outstanding grinding efficiency, particularly when dealing with various production materials. According to statistics, when starting the rotating body of a large ball mill, cracks may appear on the cylinder wall owing to the working environment, and if not detected in time, these cracks may expand. If not addressed in a timely manner, the rotating ball mill body

section can break abruptly, causing an unexpected stop in the processing process and a production shutdown (corrective maintenance). This leads to significant economic losses and increases the risk of accidents [4].

The design of ball mills requires more advanced design methods to obtain more specific and detailed data and rigorous structural parameters [5]. The dynamic effects of the ball mill and the vibration of the system were considered [6]. Therefore, the data on vibration mode analysis of significant machine elements in the literature are insufficient owing to the lack of reliable information on dynamic loads, natural oscillation frequencies, and damping [7]. For example, in Chen et al. [8] and Men et al. [9], they propose the modal analysis employing finite elements; however, they do not consider the harmonic response of the load fluctuating in time. Therefore, it is crucial to determine the reaction of the elements to impact dynamics in the study of mechanical systems, including the study of dynamic stresses and deformations in large machines, as they are in the zone of active influence to operational loads.

This study presents an applied evaluation using finite element analysis of a ball mill used in the gold mining industry, integrating static, modal, and harmonic analyses within the same assessment framework. The contribution of this work does not lie in the development of a new finite element methodology, but rather in the application of established numerical engineering methods to characterize stress distribution, deformation patterns, and dynamic behavior under representative operating conditions. The proposed approach provides a broader basis for structural diagnosis and reliability-oriented assessment of the mill shell, especially by combining static strength verification with vibrational response analysis. In this regard, the study aims to support maintenance and design decisions in industrial practice through a structural–dynamic interpretation of the system.

2. Materials and methods

2.1. 3D model of the ball mill

The analyzed system corresponds to a ball mill used for grinding gold ore. The complete machine includes the mill shell, electric motor, speed reducer, ring gear, bearings, liners, grinding media (balls), and support structure (see Fig. 1). In this work, the structural evaluation focuses on the mill body (shell and end caps), as this component concentrates the main response of stresses and deformations associated with the transmitted loads and vibratory effects.

The mill is powered by an electric motor running at 1800 rpm through a reducer, and the transmission system delivers rotational movement to the gear coupled to the

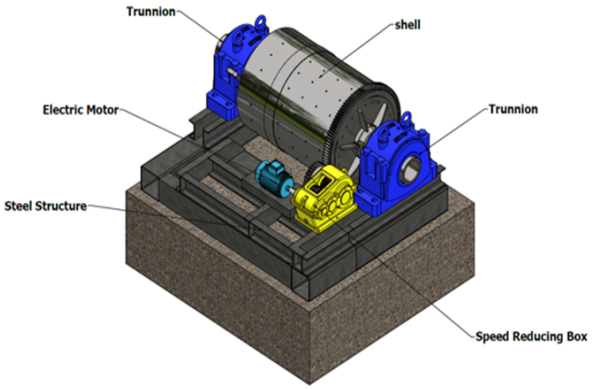

Fig. 1. Simplified ball mill

shell. To avoid ambiguity, the revised version explicitly distinguishes: (i) motor speed, (ii) output speed of the transmission, (iii) shell operating speed, and (iv) shell critical speed. The critical speed of the shell. The critical speed was calculated using Eq. (1). This critical speed (rpm) is inversely proportional to the inside diameter of the ball mill and is calculated using eq.1 [10, 11]. In this expression, n_c represents the shell critical speed (rpm) and D_{int} the internal diameter of the ball mill (m) (see Fig. 2).

$$n = \frac{42.3}{\sqrt{D_{int}}} \tag{1}$$

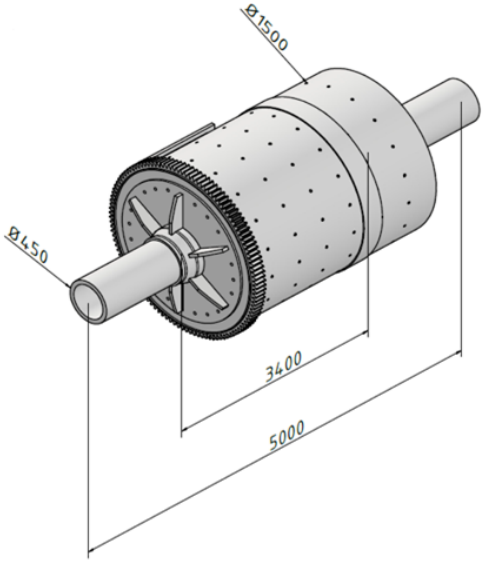

Fig. 2. Overall dimensions of the ball mill shell

Based on the calculated critical speed of 34.05 rpm, the operating speed of the shell adopted in this study was set at

Table 1. Mechanical properties of the ball mill body base material [12–16]

Steel	Yield strength (MPa)	Modulus of elasticity (GPa)	Ultimate tensile strength (MPa)	Poisson ratio	Density (kg/m^3)
A572 GR 50	345	200	450	0.26	7800

55% of the critical speed, resulting in a value of 18.73 rpm. This value falls within the operating range commonly reported for ball mills (50–70% of the critical speed), therefore representing a subcritical and technically acceptable condition [10]. To maintain consistency in the dynamic analyses, the operating speed of the shell was also expressed in frequency units using Eq. (2)

$$f_{op} = \frac{n_{op}}{60} \tag{2}$$

where n_{op} is the operating speed (rpm) and f_{op} is the operating frequency (Hz). Consequently, the adopted speed of 18.73 rpm corresponds to 0.312 Hz. This distinction is important, as the resonance evaluation is based on comparing the operating frequency with the natural frequencies obtained in the modal analysis.

In Fig. 2, the general geometry of the mill shell is shown, including the cylindrical body, end caps, and trunnion areas. All the structural connections of the assembly were modeled as bolted joints in the CAD stage. The geometry was created in Autodesk Inventor and exported to ANSYS for numerical simulation. The base material of the mill body was ASTM A572 GR. 50, so it is a strong material with good mechanical properties, economical, and widely used in the industry. The mechanical properties of the steel are listed in Table 1.

2.2. Finite element model, assumptions, and boundary conditions

The three-dimensional model generated in Inventor was imported into ANSYS for structural and dynamic analysis. The finite element model was built to evaluate the hull's behavior under static and harmonic loads, and to identify its natural modes of vibration. To make the numerical model computationally efficient without losing engineering representativeness, the following assumptions were adopted:

1. The material of the shell (ASTM A572 Gr.50) was considered homogeneous, isotropic, and linearly elastic.
2. The analyses were carried out under the assumption of small deformations.
3. The bolted assembly was represented by the overall structural continuity of the mill shell assembly (without detailed modeling of threads/local contacts), since the aim of the study is the global structural response of the mill shell.
4. The applied loads were represented as equivalent external actions (force and torque) associated with the considered operating condition.
5. In the modal analysis, damping and external excitation were disregarded, as is customary in the extraction of free, undamped vibration modes.

These assumptions are consistent with the scope of the work, which corresponds to an applied structural-dynamic evaluation of the mill shell, and not to a local analysis of contacts or nonlinearities in joints.

2.2.1. Meshing strategy

The mesh was refined iteratively and evaluated through successive simulations in order to verify the numerical stability of the main response variables. The final discretization was carried out using solid tetrahedral elements and consisted of 331,924 nodes (see Fig. 3a), which proved suitable for the static and dynamic analyses developed in this research. Additionally, the mesh achieved an average quality of 0.91 and, according to Wu et al. [17], a minimum element size of 0.7 was adopted as an acceptable criterion, thus confirming the quality of the discretization achieved. In addition to the meshed model, a mesh convergence plot was included (see Fig. 3b) to demonstrate the stabilization of the monitored outputs (maximum deformation and maximum von Mises stress) as the mesh density increased. This result supports the selection of the final mesh and strengthens the traceability and reliability of the numerical model.

2.2.2. Boundary conditions and load application

For the finite element model, specific boundary conditions were defined according to the type of analysis, as shown in Fig. 4. In all cases, the representation of the mill's support points was maintained by applying a cylindrical support condition in the trunnion region, in order to replicate the structural constraint of the real system and prevent rigid body movements of the model. In the static structural analysis (Fig. 4a), in addition to the support, a displacement condition was considered at the opposite end, as well as the simultaneous action of a force of 18,360 N, corresponding to the live load of the material entering the mill, and a

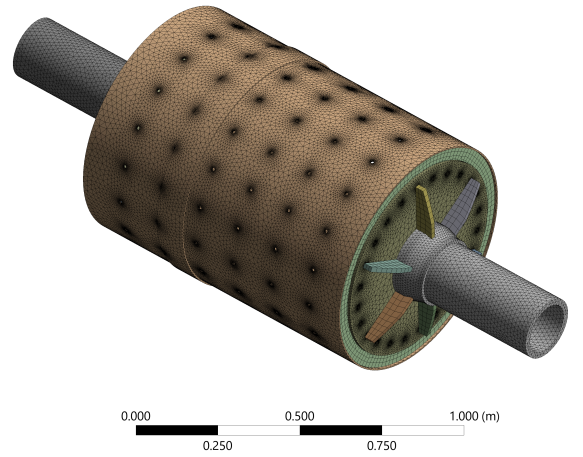

(a) Finite element discretization

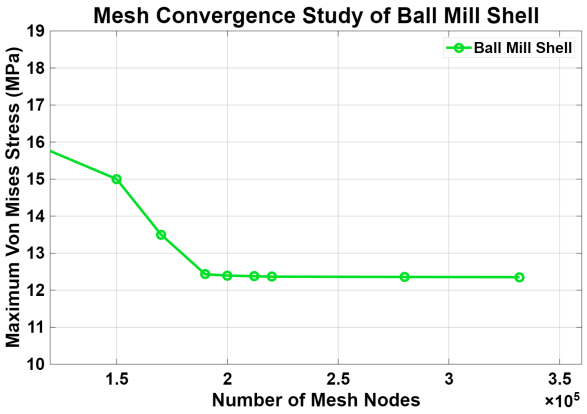

(b) Convergence curve of maximum stress

Fig. 3. Finite element discretization and mesh convergence assessment

second force of 20,000 N, associated with the equivalent permanent load of the lining and accessories. Additionally, the effect of standard gravity ($9.8066\ \mathrm{m/s^2}$) was included, and a torsional moment of 500 N · m was applied around the axis of rotation of the shell. To improve load traceability, the equivalent force and torsional moment can be related through the power transmitted and the angular velocity of the system, as follows:

$$T = \frac{P}{\omega}, \qquad \omega = \frac{2\pi n}{60} \tag{3}$$

where P is the transmitted power, ω is the angular velocity, n is the rotational speed (rpm), and r_e is the effective radius of load application. Together, these actions were imposed to provide a simplified representation of the mill's overall operating state and to assess the distribution of strains and stresses in the main cylindrical body.

For the harmonic response analysis (Fig. 4b), the same support conditions were maintained, but the excitation

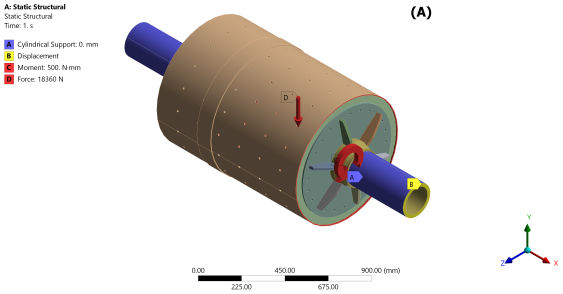

(a) Static analysis

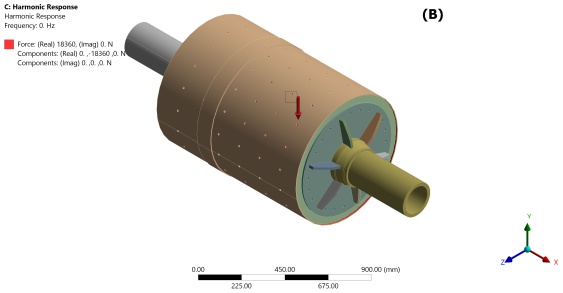

(b) Harmonic analysis

Fig. 4. The figures show the boundary conditions of the ball mill shell

was modeled solely by an equivalent sinusoidal force of 18,360 N applied in the negative direction of the Y-axis, since this load represents the variable component associated with the processed material. In contrast, the 20,000 N load was not considered as harmonic excitation, as it corresponds to a permanent system load whose effect is more appropriately represented in the static analysis. Meanwhile, in the modal analysis, only the model's support points were considered, without including external forces, gravity, torsional moment, or harmonic excitation, since this stage aims to identify the natural frequencies and the inherent mode shapes of the shell based on a free, undamped vibration formulation.

2.3. Governing equations and numerical analysis

2.3.1. Static structural analysis

Static analysis was used to determine the distribution of stresses, the strain field, and the safety factor of the mill shell under the equivalent operating load. ANSYS solves the linear static equilibrium problem in matrix form as:

$$[K]\{u\} = \{F\} \tag{4}$$

where $[K]$ is the global stiffness matrix, $\{u\}$ is the displacement vector, and $\{F\}$ is the external load vector [18].

The stress state was evaluated using the von Mises equivalent stress criterion (maximum distortion energy

theory), which is appropriate for ductile metallic materials such as ASTM A572 Gr.50 steel. From this stress field, the strain distributions and the safety factor were obtained.

2.3.2. *Modal analysis*

Modal analysis was carried out to identify the natural frequencies and mode shapes of the mill shell. In this stage, 12 vibration modes were extracted [19, 20], and damping, speed-dependent effects, and external forces were neglected [8, 21–23]. The undamped free vibration problem is solved as follows:

$$\left([K] - \omega_n^2[M]\right)\{\phi_n\} = 0 \tag{5}$$

where $[M]$ is the mass matrix, ω_n is the natural circular frequency of mode n, and $\{\phi_n\}$ is the corresponding mode shape vector. This analysis provides the fundamental dynamic characteristics of the hull and serves as a basis for interpreting the harmonic response and the risk of resonance.

2.3.3. *Harmonic response analysis*

The harmonic analysis was carried out using the modal superposition method to evaluate the steady-state response of the hull under sinusoidal excitation [24–26]. The forced vibration equation is:

$$[M]\{\ddot{u}\} + [C]\{\dot{u}\} + [K]\{u\} = \{F(t)\} \tag{6}$$

where $[M]$, $[C]$, and $[K]$ are the mass, damping, and stiffness matrices, respectively, and $\{F(t)\}$ is the time-varying harmonic load.

For a harmonic excitation of the type:

$$F(t) = F_0 \sin(\omega t) \tag{7}$$

the response in the frequency domain was evaluated within a defined range to obtain the displacement and stress amplitudes as a function of the excitation frequency. In this study, the same support configuration used in the static analysis was maintained, and a dynamic force of 18,360 N was applied in the negative direction of the Y axis (Fig. 4).

3. Results and discussion

3.1. Static analysis of the ball mill body

The global structural response, the distribution of deformations and stresses, allows for the identification of the mill's mechanical behavior under load, and was obtained using the simulation software Ansys. In Fig. 5, the maximum deformation reaches 0.04667 mm, with a red color gradient observed in the region of the mill cover, indicating the area of greatest displacement. On the other hand, Fig. 6 shows that the maximum von Mises stress is 12.351 MPa, located at the edge of the mill body's cover, due to stress concentration in this area. These results show that the highest values are concentrated in regions with geometric discontinuities, while the overall behavior of the shell remains stable under the applied load condition.

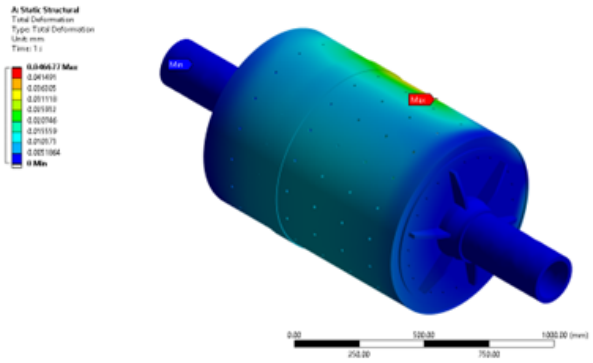

Fig. 5. Maximum ball mill shell deformation

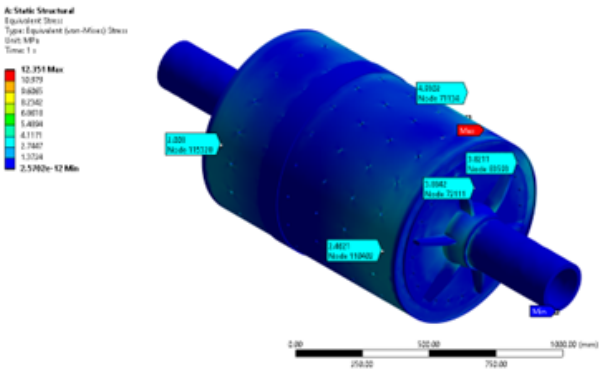

Fig. 6. Maximum ball mill shell stresses

Consequently, based on the relationship between the maximum stress obtained and the yield strength of the material, a safety factor of 27.9 was determined, as shown in Fig. 7. This value indicates that the material operates within permissible limits. However, beyond merely meeting the design criterion, this high safety factor suggests that the structure functions within the elastic regime, providing a significant structural margin against the evaluated loads. We concur with the findings reported in Dong and Li [4], where critical areas in the hollow shaft and the mill cover are identified, associated with stress concentrations.

The levels of stress and deformation obtained indicate that the structure presents adequate overall stiffness, which helps to limit excessive deformations during the equipment's operation. This behavior promotes the durability of the equipment and reduces the likelihood of fatigue

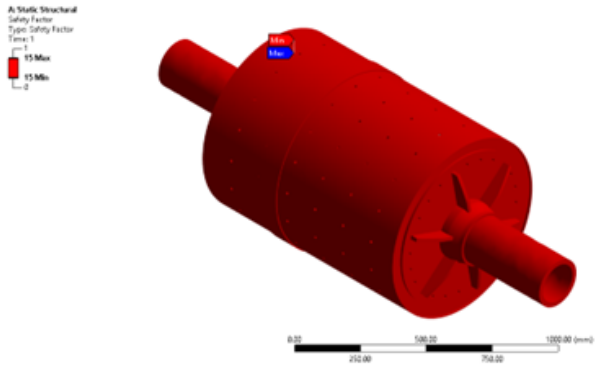

Fig. 7. Ball mill shell safety factor

damage initiation under normal operating conditions. In comparison with Dong and Li [4], who reported higher stress concentrations, the values obtained in this study are lower, which can be attributed to differences in geometry, boundary conditions, and load representation, resulting in a more uniform stress distribution in the housing.

3.2. Harmonic analysis of the ball mill body

Under sinusoidal dynamic excitation conditions, the stresses and strains reveal a moderate response from the system. The maximum stress reaches 0.155 *MPa* and is located in the central area of the mill body, near the door, where the influence of the load is most significant (see Fig. 8(A)). Additionally, the maximum strain is 0.001029 mm (see Fig. 8(B)), which is considerably lower than that obtained in the static analysis. This difference indicates that the system's dynamic response remains limited and does not show significant amplification of stresses or displacements.

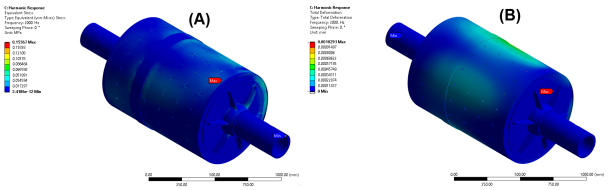

Fig. 8. Harmonic analysis of the ball mill body (A) stresses, (B) deformations

When evaluating the behavior in the frequency domain, the amplitude–frequency relationship displays peaks around 166 Hz and 410 Hz, with the maximum value occurring near 400 Hz (Fig. 9). However, these frequencies are far above the operational frequency of the mill (0.312 Hz), indicating that there is no correlation with the actual operating conditions. This behavior is consistent with vibration theory, where resonance occurs only when the excitation frequency approaches the natural frequencies of the system [27].

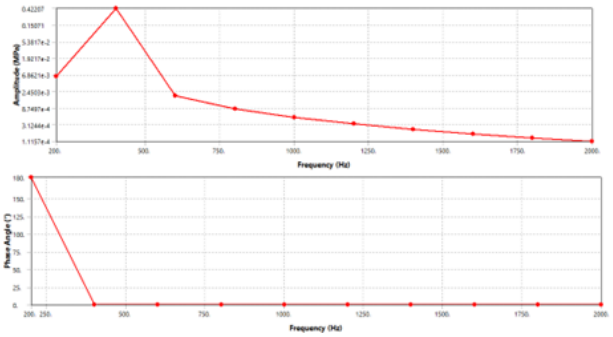

Fig. 9. Plots of the results of the ball mill harmonic analysis

From an operational and reliability perspective, the system's ability to dissipate vibrational energy without generating critical responses constitutes an important aspect of dynamic performance. This behavior prevents amplification phenomena that could compromise the structural integrity of the mill. Likewise, the fact that deformations and stresses remain within the permissible limits of the material helps reduce the risk of progressive degradation and long-term fatigue damage, reinforcing the stability and reliability of the system under real operating conditions.

3.3. Modal analysis of the ball mill body

The modal analysis results obtained in Ansys, the characterization of the natural frequencies andvibration modes allows for understanding the inherent dynamic behavior of the structure. The modes hapes shown inFig. 10(A) and Fig. 10(B), along with the values summarized in Table 2, demonstrate that the natural frequency increases with the mode order. Among the 12 modes evaluated, modes 4 and 5 exhibit the highest participation factors, making them the most representative of the system. Mode 4 (261.44 Hz) corresponds to a circumferential mode, while mode 5 (277.64 Hz) is associated with a global bending mode of the structure

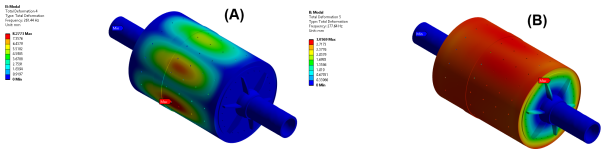

Fig. 10. Modal analysis and vibration modes of ball mill body. (A) Vibration mode 4 with frequency 261.44 Hz. (B) Vibration mode 5 with natural frequency 277.64 Hz

In relation to the actual operating conditions, the comparison between the mill's operating frequency (0.312 Hz)

Table 2. Modal vibration types of the ball mill shell

Mode	Frequency (Hz)	Vibration Type
1	218.56	Axial mode
2	222.25	Orthogonal global bending mode
3	251.87	Circumferential bending (low order)
4	261.44	Circumferential shell mode
5	277.64	Global bending mode
6	286.53	Higher-order circumferential mode
7	299.65	Coupled axial–circumferential mode
8	333.05	Local shell bending mode
9	355.93	Higher-order bending mode
10	399.80	Complex circumferential mode
11	418.06	Local axial–torsional mode
12	424.05	Combined high-order axial–circumferential mode

and the obtained natural frequencies shows a significant separation between both values. This difference implies a very low probability of resonance during normal operation, which is a key indicator of dynamic stability. In accordance with Rishmany and Imad [10], the operating frequencies of this type of equipment are usually kept away from the natural frequencies. Nevertheless, the analysis conducted is limited to the first 12 vibration modes considered in the analysis.

When comparing these results with the specialized literature, Wójcicki et al. [28] report lower natural frequencies when considering the complete system, including the foundation and supports. This difference is consistent with the scope of the present study, which focuses exclusively on the mill shell. Likewise, compared to Dong and Li [4], who identify higher stress concentrations in critical areas, the results obtained in this work suggest a more uniform structural behavior and a more efficient load distribution, which contributes to improving the dynamic performance of the system under the evaluated conditions.

As a future line of research, it is recommended to assess load variability based on the non-homogeneous material distribution within the shell, as well as to examine the impact of internal liner wear on the system's strength. Additionally, conducting a long-term structural fatigue analysis would be relevant to determine the effective life of the mill under cyclic operating conditions.

4. Conclusion

This study mainly considered the shell of the ball mill as the research object, carried out stress analysis on the cylinder body, and used the finite element analysis method to optimize the design. By calculating the working state of the ball mill cylinder, it was found that the stress in the working state and the steady state were the same. Under normal working conditions, the force in the ball mill cylinder is more significant than that in the static state of the full load. According to the finite element model analysis, the maximum static load of the ball mill was 12.35 *MPa*, and the maximum deformation was 0.04667 *mm*, which met the production requirements of the ball mill. Modal analysis was used to determine the critical vibration modes of the ball mill. Vibration mode 4 exhibited circumferential behavior, where alternating deformations were observed along the cylinder casing, with a natural frequency of 261.44 Hz. However, vibration mode 5 corresponds to an bending mode, characterized by vibrations predominantly along the longitudinal axis of the mill, with a natural frequency of 277.64 Hz. This is the highest mass participation factor and the highest value of dynamic responses. Compared with an operating frequency of 0.312 Hz (18.7 *rpm*), the natural frequencies do not coincide. Therefore, there was no risk of resonance. Finally, the effect of the sinusoidal force originating from the ore-crushing process was investigated using harmonic analysis. The results revealed that the stress and deformation values remained within the permissible parameters, highlighting the robustness of the structure against such loads. In addition, no resonance was observed in the ball mill, underlining the stability and reliability of the equipment even under intense dynamic loading conditions.

References

[1] P. V. Malyarov, (2017) *"Upon ball mill combination liner design"* **Obogashchenie Rud** (3): 10–14. DOI: 10.17580/or.2017.03.02.

[2] T. Yoshida, F. Kuratani, T. Ito, and K. Taniguchi. "Vibration characteristics of an operating ball mill". In: *Journal of Physics: Conference Series*. ***1264***. 1. 2019. DOI: 10.1088/1742-6596/1264/1/012016.

[3] S. Banisi and M. Hadizadeh, (2007) *"3-D liner wear profile measurement and analysis in industrial SAG mills"* **Minerals Engineering *20***(2): 132–139. DOI: https://doi.org/10.1016/j.mineng.2006.07.008.

[4] Y. Dong and Q. Li, (2018) *"Stress analysis and optimization design & research of the large ball mill cylinder"* **Chemical Engineering Transactions *66***: 709–714. DOI: 10.3303/CET1866119.

[5] Y. Li, Q. Xiao, Y. Fu, S. Jin, G. Wang, M. Wang, B. Sun, H. Tian, X. Liu, and J. Tian, (2025) *"An innovative theoretical model for optimizing ball diameter in tumbling mills"* **Minerals Engineering *233***: 109635. DOI: 10.1016/j.mineng.2025.109635.

[6] P. Huang, M.-p. Jia, and B.-l. Zhong, (2009) *"Investigation on measuring the fill level of an industrial ball mill based on the vibration characteristics of the mill shell"* **Minerals Engineering 22**(14): 1200–1208. DOI: https://doi.org/10.1016/j.mineng.2009.06.008.

[7] , (2025) *"Digital simulation of rock grinding process in ball mill"* **Scientific Reports 2025 15:1 *15***: 45653–. DOI: 10.1038/s41598-025-30289-7.

[8] L. T. Chen, Y. J. Xue, Y. Liu, and J. S. Li. "Modal analysis of oversize ball mill tube based on ANSYS". In: *Advanced Materials Research*. ***889-890***. 2014, 62–65. DOI: 10.4028/www.scientific.net/AMR.889-890.62.

[9] Q. Y. Men, G. W. Cheng, and Y. Han. "Modal analysis of ball mill rotator based on FEM technique". In: *Advanced Materials Research*. ***199-200***. 2011, 1451–1456. DOI: 10.4028/www.scientific.net/AMR.199-200.1451.

[10] J. Rishmany and R. Imad, (2023) *"Finite Element and Multibody Dynamics Analysis of a Ball Mill Glass Crusher"* **Modelling and Simulation in Engineering *2023***: DOI: 10.1155/2023/1905702.

[11] H. Watanabe, (1999) *"Critical rotation speed for ball-milling"* **Powder Technology *104***(1): 95–99. DOI: https://doi.org/10.1016/S0032-5910(99)00031-5.

[12] H. C. Ho, M. Xiao, Y. F. Hu, Y. B. Guo, K. F. Chung, M. C. H. Yam, and D. A. Nethercot, (2020) *"Determination of a full range constitutive model for high strength S690 steels"* **Journal of Constructional Steel Research *174***: DOI: 10.1016/j.jcsr.2020.106275.

[13] H. U. Sajid and R. Kiran, (2018) *"Influence of high stress triaxiality on mechanical strength of ASTM A36, ASTM A572 and ASTM A992 steels"* **Construction and Building Materials *176***: 129–134. DOI: 10.1016/j.conbuildmat.2018.05.018.

[14] S.-H. Lee and B.-J. Choi, (2021) *"Mechanical properties of astm a572 grades 50 and 60 steels at high temperatures"* **Applied Sciences (Switzerland) *11***(24): DOI: 10.3390/app112411833.

[15] Z. Guo, X. Jia, and W. Qiao, (2019) *"Mechanical Properties of Butt Weldments Made with Q345B Steel and E5015 Electrodes at Different Temperatures"* **Journal of Materials in Civil Engineering *31***(9): DOI: 10.1061/(ASCE)MT.1943-5533.0002845.

[16] T. M. D. Borba, R. S. Oliveira, H. R. Gama, M. F. O. Caizer, and L. O. Turani, (2017) *"Weldability evaluation of sincron EN 10025-4 S355M steel applied in wind tower manufacturing welding with high efficiency process"* **Soldagem e Inspecao 22**(4): 413–428. DOI: 10.1590/0104-9224/SI2204.12.

[17] M. Wu, J. Mu, L. Zhuang, Y. Kong, X. Zhou, L. Zhuang, M. Wu, Y. Kong, X. Zhou, and J. Mu, (2020) *"Fatigue analysis of injector body based on ANSYS workbench"* **Vibroengineering Procedia *30***: 193–198. DOI: 10.21595/vp.2019.21183.

[18] X. Yang, C. Zhang, and L. Zhou, (2023) *"Static analysis and optimization design of a special-shaped rod of the crab-like robot based on ANSYS Workbench"* **Journal of Physics: Conference Series *2459***: 012136. DOI: 10.1088/1742-6596/2459/1/012136.

[19] G. Z. Villarroel, R. V. Martinez, J. R. C. Grandon, and S. P. Gutiérrez, (2023) *"A Systematic Procedure for Design and Structural Mechanical Analysis: A Case Study for Construction of a Buggy"* **International Journal of Mechanical Engineering and Robotics Research *12***(6): 362–377. DOI: 10.18178/ijmerr.12.6.362-377.

[20] E. Marliana and I. Ismail, (2021) *"Dynamics characteristics analysis on shaft sprocket assembly of rake conveyor"* **Trends in Sciences *18***(19): DOI: 10.48048/tis.2021.11.

[21] W. Tanaś, J. Szczepaniak, J. Kromulski, M. Szymanek, J. Tanaś, and M. Sprawka, (2018) *"Modal analysis and acoustic noise characterization of a grain crusher"* **Annals of Agricultural and Environmental Medicine *25***(3): 433–436. DOI: 10.26444/aaem/87154.

[22] Y. Wang, G. Tan, B. Yang, and C. Wang. "The Finite Element Analysis and Optimization on a Special Vehicle". In: *SAE Technical Papers*. ***2015-April***. April. 2015. DOI: 10.4271/2015-01-0473.

[23] M.-L. Hao and G.-J. Cheng. "Modal analysis based on finite element jaw crusher rotor". In: *Applied Mechanics and Materials*. ***599-601***. 2014, 547–550. DOI: 10.4028/www.scientific.net/AMM.599-601.547.

[24] Z. Tang, H. Wu, Z. Wu, D. Jia, and Y. Fu, (2023) *"Modal analysis and harmonic response analysis of energy-absorbing and anti-scouring columns"* **Frontiers in Earth Science *11***: DOI: 10.3389/feart.2023.1126120.

[25] S. Perumal, R. Swaminathan, and M. Christensen. "Forced Vibration Harmonic Response Analysis of Semi-mobile Crusher Station". In: *Lecture Notes on Multidisciplinary Industrial Engineering*. ***Part F249***. 2020, 157–169. DOI: 10.1007/978-981-13-8468-4_14.

[26] L. O. B. Coronado, L. I. M. Ballesteros, E. J. T. Geraldo, A. M. Buison, U. B. Ante, J. B. L. Padaca, V. Sarmiento, D. D. A. Florante, J. A. V. Garcia, and F. P. Liza. "Finite Element Modal Analysis and Harmonic Response Analysis of a 3D Printed Vibration Sensor Enclosure". In: *2021 IEEE 13th International Conference on Humanoid, Nanotechnology, Information Technology, Communication and Control, Environment, and Management, HNICEM 2021*. 2021. DOI: 10.1109/HNICEM54116.2021.9731919.

[27] S. S. Rao. *Mechanical vibrations*. Pearson Education, Inc., 2017, 1118.

[28] Z. Wójcicki, J. Grosel, W. Sawicki, K. Majcher, and W. Pakos. "Experimental (OMA) and numerical (FEM) modal analysis of ball mill foundations". In: *Procedia Engineering*. ***111***. 2015, 858–863. DOI: 10.1016/j.proeng.2015.07.159.